Food Hydrocolloids 145 (2023) 109139

Contents lists available at ScienceDirect

Food Hydrocolloids

journal homepage: www.elsevier.com/locate/foodhyd

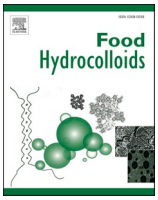

Preparation, physicochemical properties, and formation mechanism of quinoa self-assembled peptide-based hydrogel

Xin Fan [a,b,f], Huimin Guo [a,d,e], Aurore Richel [e], Lizhen Zhang [c], Chenghong Liu [d], Peiyou Qin [a,b,**], Christophe Blecker [f,***], Guixing Ren [a,b,c,*]

[a] Key Laboratory of Quality Evaluation and Nutrition Health of Agro-Products, Ministry of Agriculture and Rural Affairs, Institute of Crop Sciences, Chinese Academy of Agricultural Sciences, Beijing 100081, China
[b] Key Laboratory of Coarse Cereal Processing, Ministry of Agriculture and Rural Affairs, School of Food and Biological Engineering, Chengdu University, Chengdu 610106, China
[c] Key Laboratory of Chemical Biology and Molecular Engineering of Ministry of Education, School of Life Science, Shanxi University, Taiyuan, 030006, China
[d] Shanghai Key Laboratory of Agricultural Genetics and Breeding, Biotechnology Research Institute, Shanghai Academy of Agricultural Sciences, Shanghai 201106, China
[e] Laboratory of Biomass and Green Technologies, Gembloux Agro-Bio Tech, University of Liège, Gembloux, Belgium
[f] Department of Food Science and Formulation, Gembloux Agro-Bio Tech, University of Liège, Gembloux, Belgium

ARTICLE INFO

Keywords:
Quinoa protein
Enzymatic hydrolysis
Gelation
Rheological property
Microstructure
Molecular characteristics

ABSTRACT

Currently, self-assembly peptides with hydrogel properties that are used in various applications are being chemically synthesized. These peptides not only have safety and environmental problems but are also expensive and cumbersome to prepare. The present study established a convenient and efficient method for producing plant-based peptides with decent gel-forming ability from quinoa proteins. After alkaline protease treatment, hydrogels made with quinoa protein hydrolysis exhibited potent self-assembly capacity, enhanced gel hardness, and improved rheological properties. Moreover, the microstructure results revealed that the quinoa peptide hydrogels had regular, uniform, and interconnected porous structures. These observations were primarily attributed to the hydrogen bonding force and hydrophobic aggregation caused by hydrophobic group exposure. Amino acid and proteomics analysis suggested that the amino acid composition and sequence of quinoa peptides significantly influenced the formation of self-assembled hydrogels. Overall, this study provided a cost-effective approach to improve the gelling ability of quinoa protein and could potentially replace the use of chemically synthesized peptides in various applications, laying the theoretical basis for the development of novel natural plant-based foods.

1. Introduction

With the rapid growth of the human population and intensifying greenhouse effect, plant-based proteins are considered a promising alternative to meet the growing demand for nutritional food and reduce the consumption of animal-origin food. A reasonable combination intake of plant proteins or as a main food ingredient can ensure adequate nutrition for the human body to maintain a healthy state. Soy and pea proteins are the most well-known plant protein sources. To provide more plant proteins with high nutritional value and quality, it is necessary to deepen mining and research on other superior plant proteins. Quinoa—a new food and emerging protein source—has received widespread attention because of its high protein content and well-balanced amino acid compositions (McClements, Newman, & McClements, 2019). Additionally, quinoa has a high content of essential amino acids, primarily lysine, methionine and cysteine, and is gluten-free (Elsohaimy, Refaay, & Zaytoun, 2015), making it highly valuable in plant-based protein products and appealing to broader consumers.

Enzymatic hydrolysis is recognized as a promising and effective approach for improving the functional properties and nutritional value of proteins. Moreover, gelation is believed to be one of the most crucial

* Corresponding author. Institute of Crop Sciences, Chinese Academy of Agricultural Sciences, Beijing 100081, China
** Corresponding author. Key Laboratory of Quality Evaluation and Nutrition Health of Agro-Products, Ministry of Agriculture and Rural Affairs, Institute of Crop Sciences, Chinese Academy of Agricultural Sciences, Beijing 100081, China
*** Corresponding author. Department of Food Science and Formulation, Gembloux Agro-Bio Tech, University of Liège, Gembloux, Belgium
E-mail address: renguixing@caas.cn (G. Ren).

https://doi.org/10.1016/j.foodhyd.2023.109139
Received 26 April 2023; Received in revised form 23 July 2023; Accepted 1 August 2023
Available online 2 August 2023

techno-functionalities of proteins and is extensively used in food processing and pharmaceuticals (Gosal & Ross-Murphy, 2000). Peptides—the main products of protein enzymatic hydrolysis—have the potential to form self-assembled hydrogels, which have attracted widespread interest because of their ease of preparation, reproducibility, biodegradability, biocompatibility, and the availability of various chemical functions and structures (De Leon Rodriguez & Hemar, 2020). However, these gelation-capable peptides are mainly obtained through designed synthesis or microbial recombinant expression (De Leon Rodriguez & Hemar, 2020). It is still difficult to apply synthetic peptides to practical production applications because of their limitations, including difficulties in purification, low stability, poor dispersion, and safety issues (Yu, et al., 2022). Therefore, a safe, easily accessible, and environmentally friendly method to produce plant-based peptides with gel-forming abilities is imminent.

Although animal proteins have been suggested to have better gelation properties than plant proteins, enzymatic hydrolysis can improve the gelation properties of plant proteins by changing the ionic interactions, hydrogen bonds, and hydrophobic regions (Nieto-Nieto, Wang, Ozimek, & Chen, 2014; Zhao, Liu, Zhao, Ren, & Yang, 2011). For instance, oat protein isolates exhibited enhanced gel-forming abilities after hydrolyzing with flavourzyme and trypsin at pH 9 by adjusting the electrostatically repulsive force and the hydrophobic attractive force (Nieto-Nieto, et al., 2014). Similarly, compared to pea protein, the gelling capacity of pea protein hydrolysate increased after alcalase treatment followed by heating at 85 °C for 10 min (Chen & Campanella, 2022). However, in a recent study on the gelation properties of quinoa protein, the quinoa peptide gels were formed in an acidic condition (pH < 3), and their gel strength decreased with the raising pH (Galante, De Flaviis, Boeris, & Spelzini, 2020). Although several plant-based hydrogels have been obtained through enzymatic hydrolysis, the formation conditions require constant adjusting and are cumbersome to apply in food processing. Furthermore, these studies have mainly focused on the structural properties and did not investigate the effect of small molecular weight plant-based peptides, which are more similar to synthetic self-assembled peptides, on hydrogel formation. Therefore, the present study provided a simple and efficient method for producing self-assembled hydrogels via mild alcalase hydrolysis of quinoa proteins. We determined the physicochemical properties of quinoa peptide hydrogels, including molecular weight, degree of hydrolysis, gel hardness, rheological properties, and surface hydrophobicity. Moreover, the potential gelation mechanism of the quinoa hydrogels was elucidated based on the results of particle size distribution, zeta potential, free sulfhydryls, Fourier transform infrared spectroscopy, scanning electron microscopy, and amino acid and proteomics analysis. Our study provided the rationale for the development of novel, green, and safe plant-based protein foods.

2. Materials and methods

2.1. Materials

Quinoa seeds (*Mengli-I*) were obtained from the Inner Mongolia Yiji Biotechnology Company (Ulanqab, China). Sodium hydroxide (NaOH), hydrochloric acid (HCl), and *n*-hexane were obtained from Sinopharm Chemical Reagent Co. Ltd. (Shanghai, China). Alcalase (≥200,000 U/g) was obtained from Novozyme (Beijing, China).

2.2. Quinoa protein, quinoa protein hydrolysates, and hydrogel preparation

QP extraction was conducted according to a previous method (Galante, et al., 2020) with some modifications. Quinoa flour was dispersed in distilled water (10%, *w/v*). The suspension was stirred for 2 h at room temperature and then centrifuged at 6000 g for 30 min. The supernatant was adjusted to pH 4 by adding 1 M HCl to precipitate the proteins and then centrifuged at 6000 g for 30 min. The precipitate was resuspended in water, adjusted to a pH of 7.0, and freeze-dried. The obtained powder was denoted as QP. QP suspension (5%, *w/v*) was hydrolyzed with alcalase at a QP:alcalase ratio of 200:3 (*w/w*) at pH 8.0 and 55 °C. Samples were collected at different hydrolysis intervals (0, 15, 30, 60, 90, 120, 150, and 180 min). The 180-min alcalase hydrolysate was further freeze-dried and termed QPH.

The hydrogel was prepared by mixing the freeze-dried QP or QPH powder with deionized water at a pH of 7.0, completely oscillating for 1 min, and allowed to stand for 10 min at room temperature.

2.3. Degree of hydrolysis determination, sodium dodecyl sulfate-polyacrylamide gel electrophoresis (SDS-PAGE), and molecular weight

In this study, the degree of hydrolysis (DH) was determined according to the method of Adler-Nissen (1979) with slight modifications. QPH samples were added to sodium phosphate buffer (0.2 M, pH 8.2). TNBS reagent (0.1% *w/v*) was added to start the reaction and incubated at 50 °C for 1 h. After incubation, 0.1 N HCl was added to stop the reaction. The absorbance was measured at 340 nm.

The QP hydrolysis was verified using SDS PAGE. The samples were mixed with a loading buffer (2 × , Bio-Rad, USA; 1:1 (v/v)), boiled at 100 °C for 10 min, and rapidly cooled on ice. The samples were loaded onto a Mini-protein TGX precast gel (Bio-Rad, USA) and the gel was subjected to electrophoresis at 120 V under reducing conditions on a Mini-PROTEAN 3 Cell system (Bio-Rad, USA). The protein bands were visualized by staining with Coomassie R250 brilliant blue (Biorigin, Beijing, China). A colour Prestained Protein Marker (Genstar, Beijing, China) was used as the molecular weight standard.

The molecular weight (Mw) distribution was determined using a Waters high-performance liquid chromatography (Waters, Milford, MA, USA) equipped with a refractive-index detector (Waters 2414). The samples were separated through a PL Aqua gel-OH mixed-H 8 μm column (Agilent Technologies, Santa Clara, CA, USA) at 30 °C. The mobile phase consisted of 0.2 M $NaNO_3$ and 0.01 M NaH_2PO_4 aqueous solution (pH 7.0) at a rate of 1 mL/min, and 20 μL of 5 mg/mL sample was injected into the high-performance liquid chromatography system. A calibration curve was obtained using narrow-distribution polyethylene glycol of known molecular weight to obtain the molecular weight calibration curve. Data was analyzed using gel permeation chromatography (GPC) software (Waters, Milford, MA, USA).

2.4. Texture analysis

Texture measurements were conducted using a TMS-PRO series Texture Profile Analyzer (TMS-Pro, FTC, USA). The samples were prepared in cylindrical containers (20 mm diameter × 10 mm height). The cylindrical plunger (5 mm diameter) penetrated 50% into the gel samples at a crosshead speed of 5 mm/s and a return speed of 5 mm/s with a trigger force of 49 mN. The maximum breaking force was defined as the hardness (N) of gels. Four independent replicates were measured for each sample.

2.5. Rheological properties

A Haake Mars60 rotational rheometer (Thermo Fisher, Germany) equipped with a stainless-steel parallel plate (diameter, 40 mm; gap, 1 mm) was used to measure the rheological properties of the hydrogel. The hydrogels were placed on a parallel plate for 2 min to maintain the temperature equilibrated at 25 °C before each measurement. The viscosity was detected using the steady shear mode, and the shear rates ranged from 0.1 to 100 s^{-1}. The frequency sweep measurements were performed at a constant strain of 1%, whereas the frequency varied from 0.01 to 100 Hz. The storage modulus (G′), loss modulus (G″) and loss tangent ($\tan\delta = G''/G'$) were recorded as functions of the frequency. At least three measurements were measured per sample.

2.6. Determination of particle size distribution (PSD)

The particle size distributions of QP and QPH were determined using a Malvern Mastersizer 2000 analyzer (Malvern Instruments, Worcestershire, UK) and static light scattering. The refractive indices (RI) used for the samples and dispersant were 1.52 and 1.33, respectively. The volume-weighted mean D [4, 3] represents the mean particle size. All samples were dissolved in water at a concentration of 1 mg/mL and transferred into a water-filled tank of the instrument filled with water. The samples were homogeneously dispersed in water by continuous stirring and ultrasonic. The mean particle size and particle size distribution were obtained from the software based on the diffraction of laser scattered by the sample particles. Each value was conducted in triplicate on duplicate samples at room temperature.

2.7. Scanning electron microscopic observation

Protein and peptide hydrogel microstructures were observed using scanning electron microscopy (SEM, Hitachi Corporation, Japan). All samples (12%) were frozen at −80 °C, freeze-dried using a vacuum freeze-dryer, and cut into small pieces ($2 \times 2 \times 1$ mm^3). The fracture surfaces were observed using SEM after being sputter-coated with gold.

2.8. Zeta potential

Zeta-potential was measured using a Dynamic Laser Light Scattering instrument (Zetasizer Nano-Zs, Malvern Instruments, UK) at room temperature. The freeze-dried samples were diluted in 0.1 mol/L sodium phosphate buffer (pH 7.0) at a concentration of 1 mg/mL. Four replicates were performed for each sample.

2.9. Determination of surface hydrophobicity and free sulfhydryl contents

Surface hydrophobicity was measured using 1-anilino-8-naphthalene sulfonate as a hydrophobic probe according to the method of (Zuo, et al., 2022) with minor modifications. Different hydrolysate samples were diluted to 1 mg/mL concentration with phosphate buffer (0.1 M, pH 7.0). Approximately 2 mL of each sample was mixed with 50 μL of 8.0 mM ANS solution and allowed to react for 20 min in the dark. Fluorescence intensity was detected using a Synergy HT spectrofluorometer (BIO-TEK, VT, USA) with a slit width of 5 nm. The excitation and emission wavelengths were 390 and 470 nm, respectively. The slope value of fluorescence intensity versus sample concentration was used as the index of surface hydrophobicity.

The free sulfhydryl (-SH) groups were determined using Ellman's reagent (DTNB, 5,5′-dithio-bis-(2-nitrobenzoic acid) as previously described (Beveridge, Toma, & Nakai, 1974; Yin, Tang, Wen, & Yang, 2010) with some modifications. The samples (50 mg) were dissolved in 10 mL Tris-glycine buffer containing 2 mmol/L ethylenediaminetetraacetic acid (EDTA), and then 100 μL Ellman's reagent was added. The mixed suspension was placed in the dark for 1 h at 25 °C. The mixture without a sample was used as the blank control. Absorbance was measured at 412 nm. The SH concentration was calculated using the molar extinction coefficient of 2-nitro-5-thiobenzoateat and the equation is as follows:

$$\mathrm{SH}\ (\mu\mathrm{mol/g}) = (A_{412} \times 10^6) / [(b \times \varepsilon) \times C],$$

Where A_{412} is the absorbance at 412 nm, 10^6 (μmol/mol), b (cm) is the cuvette path length, ε (14,150 L mol^{-1} cm^{-1}) is the molar extinction coefficient, and C (g/L) is the sample concentration.

2.10. Fourier transform infrared spectroscopy (FTIR)

Infrared spectra were recorded using a Shimadzu IRAffinity-1S FTIR-spectrometer (Shimadzu, Tokyo, Japan) equipped with a diamond attenuated total reflectance (ATR) attachment. The sample was mixed with KBr at a ratio of 1:100 (*w/w*) and compressed into a tablet. Measurements were performed in the 4000-600 cm^{-1} at a resolution of 4 cm^{-1} with a total of 32 scans. The sample data were analyzed using the OPUS 7.2 spectroscopy software. The secondary structure of the protein was assigned by band fitting the amide I region (1700–1600 cm^{-1}) using Omnic 8.2 software and reported as the percentage of the total peak area.

2.11. Amino acid and proteomics analysis

The amino acid composition of QPH was determined using high-performance liquid chromatography (HPLC, LC20A, Shimadzu, Japan) with pre-column phenylisothiocyanate (PITC) derivatization. Briefly, the QPH sample was dissolved in 6 M HCl and hydrolyzed for 24 h at 110 °C. The hydrolysate was dried and derivatized with PITC at room temperature for 30 min. After derivatization, the sample was detected using a reversed-phase HPLC with a UV detector (254 nm).

Mass spectrometry data were collected using an EASY-nLC 1200 HPLC system in series with a Q Exactive HF-X mass spectrometer (Thermo, MA, USA). The QPH sample was dissolved in water and centrifuged at 12,000 g for 10 min. The supernatant was filtered through a 5-kD ultrafiltration filter and desalted using a C18 column. Thereafter, the desalted peptides solution was concentrated using a centrifugal concentrator and allowed to undergo further detection. The peptide sample was loaded onto the pre-column via an autosampler and then separated through an analytical column (C18, 2 μm, 75 μm × 25 cm). The liquid chromatography method was set as follows: mobile phase A (0.1% formic acid), mobile phase B (0.1% formic acid), flow rate (300 nL/min), and the gradient employed was a 100 min linear gradient. Mass spectrometry data acquisition was performed in DAA mode with a full-scan MS (Resolution: 60,000, automatic gain control (AGC) target value: 3e6, scan range: 350–1800 *m/z*, maximum injection time: 20 ms) and 25 MS/MS scans (Resolution: 15,000, automatic gain control (AGC) target value: 2e5, maximum injection time: 50 ms). The isolation window was set to 1.6 *m/z*, the high-energy dissociation (HCD) normalized collision energy was set to 28%, and the dynamic exclusion time of repeated ion acquisition was set to 35 s.

Raw MS and MS/MS data were analyzed using Maxquant software (version 1.6.6). The database searches against the UniProt protein database were carried out using the search engine Andromeda. The search parameters were as follows: carbamidomethyl (C) was set as a fixed modification; oxidation (M) and acetyl (protein *N*-term) were used as variable modifications; the mass tolerance in MS was set to 20 ppm, the main search tolerance was set to 4.5 ppm; the MS/MS tolerance was set to 20 ppm; the identifications were filtered to acquire a 1% false discovery rate (FDR).

2.12. Statistical analysis

All measurements were conducted in duplicate or triplicate, and the experimental results were presented as mean ± standard deviations (SD). Statistical differences among means were determined using GraphPad Prism (version 9.3.0) through one-way or two-way ANOVA, and significant differences were considered at $p < 0.05$.

3. Results and discussion

3.1. Quinoa protein and its hydrolysates

According to a previously reported method, the quinoa protein yield and purity were determined to be 6.85% and 86.02%, respectively. The SDS-PAGE protein pattern showed that QP had many bands with varying levels of intensity (Fig. 1A). According to previous literature, the band with a molecular weight above 65 kDa corresponded to 7 S Globulin, and the band around 45–55 kDa was assigned to 11 S globulin (Brinegar

& Goundan, 1993; Shen, Tang, & Li, 2021). Under reduced conditions, the disulfide bonds of 11 S globulin were broken to form acidic (AS) and basic (BS) polypeptide subunits with the molecular mass of 32–39 kDa and 20–23 kDa, respectively (Abugoch, Romero, Tapia, Silva, & Rivera, 2008; Brinegar & Goundan, 1993). Additionally, the band at approximately 10 kDa corresponded to 2 S albumin (Brinegar, Sine, & Nwokocha, 1996).

To obtain quinoa peptides, QP was digested with alcalase for 180 min. The extent of protein degradation is represented by DH (Fig. 1B). QP experienced steady hydrolysis from 0 of DH at the beginning to 15% in 90 min, the 11 S globulin band quickly degraded, and the alkaline subunit of 11 S globulin gradually disappeared. As the hydrolysis degree increased, the intensity of high-molecular-weight bands decreased. When DH reached 18% after 180 min, all subunits partially disappeared. These results demonstrated that the peptide fragments were released during the hydrolysis and these quinoa peptides were less than 10 kDa. GPC results depicted that the 180-min hydrolysate had a mean Mw of 5.01 kDa, demonstrating that the peptides were released during the hydrolysate process.

3.2. Gelation of QP and its hydrolysates

According to previous studies, pH adjustment and heat treatment are identified as the main factors affecting the gelation property of QP (Galante, et al., 2020; Ruiz, Xiao, van Boekel, Minor, & Stieger, 2016). Moreover, the gel formation of QP was induced and affected by salt addition (Yang, et al., 2022). In the present study, QP did not exhibit gel-forming properties before adding alcalase. However, as hydrolysis proceeded, the solution became slightly viscous after 60 min, suggesting that the peptides might have formed organized microstructures. Subsequently, the gel properties of QPH were examined, and 10%–15% (*w/v*) of QP and QPH suspensions were prepared. As shown in Fig. 2A, no hydrogels formed of QP within the concentration range of 10%–15%. Notably, QPH formed hydrogels at 11%–15%, and 10% was the critical concentration of hydrosol to hydrogel. In contrast to a previous study, QPH with potent hydrogel-forming capacity was prepared through excessive hydrolysis. Moreover, QPH hydrogels could be obtained by dissolving QPH in water at a suitable ratio without other chemical induction steps.

As previously mentioned, QP gradually exhibited gel-forming properties with increasing DH. Therefore, the hardness variation of 12% QP during hydrolysis was determined (Fig. 2B). There was a rising trend in hardness as hydrolysis time increased. In the beginning, the hardness significantly increased more than doubled from 91.86 mN (4.68 kPa) of QP to 222.07 mN (11.31 kPa) of 15-min QPH. After that, there was a smooth uptrend of its hardness, which increased significantly to 487.52 mN (24.83 kPa) at 180 min. Furthermore, the hardness of QP and QPH at different concentrations was also measured. As shown in Fig. 2C, the texture test results showed that the hardness of QPH presented an upward trend with the increased concentration, and the breaking force was from 388.83 mN (19.20 kPa) of 10% hydrosol to 654.22 mN (33.32 kPa) of 15% hydrogel. Conversely, QP did not show appreciable changes in hardness (84.74–95.03 mN (4.32–4.84 kPa)) at each concentration of 10%–15% (Fig. 2C). These results indicate that excessive hydrolysis is an effective approach to produce quinoa peptides with potent hydrogel-forming abilities.

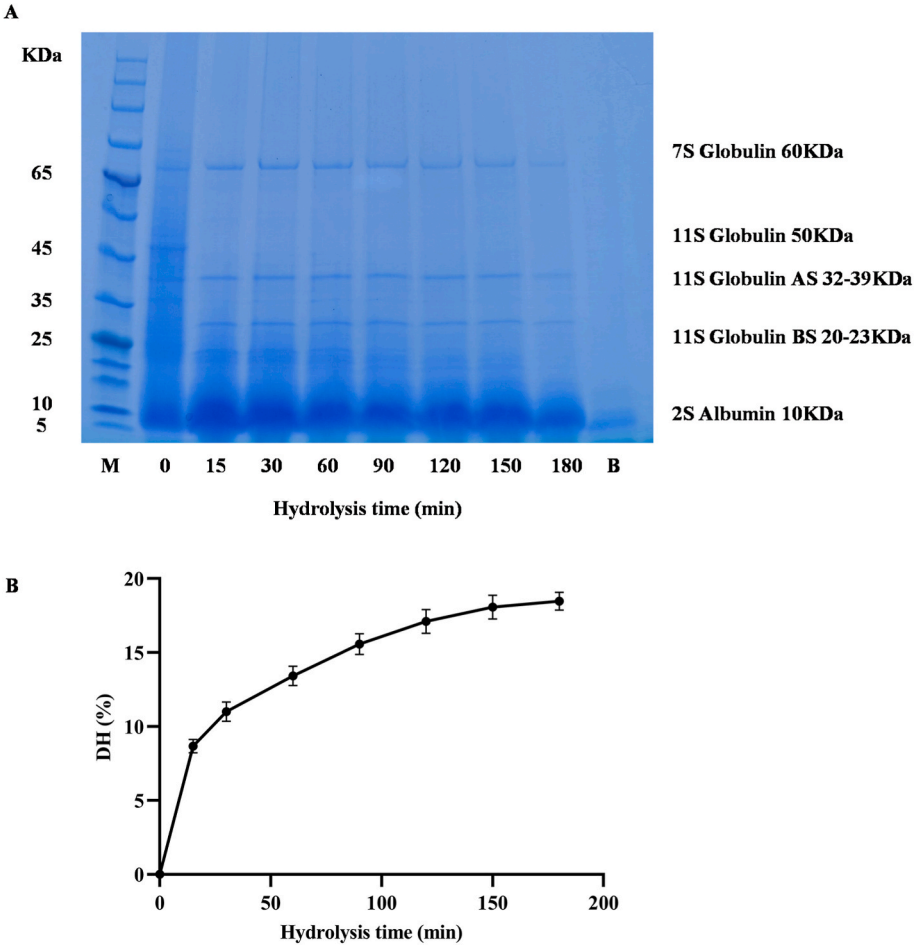

Fig. 1. (A) SDS-PAGE profiles of quinoa protein (QP) and its hydrolysates (QPH) resulting from alcalase hydrolysis at various incubation times. M: molecular weight marker; B: blank; (B) Degree of hydrolysis of QP under alcalase treatment.

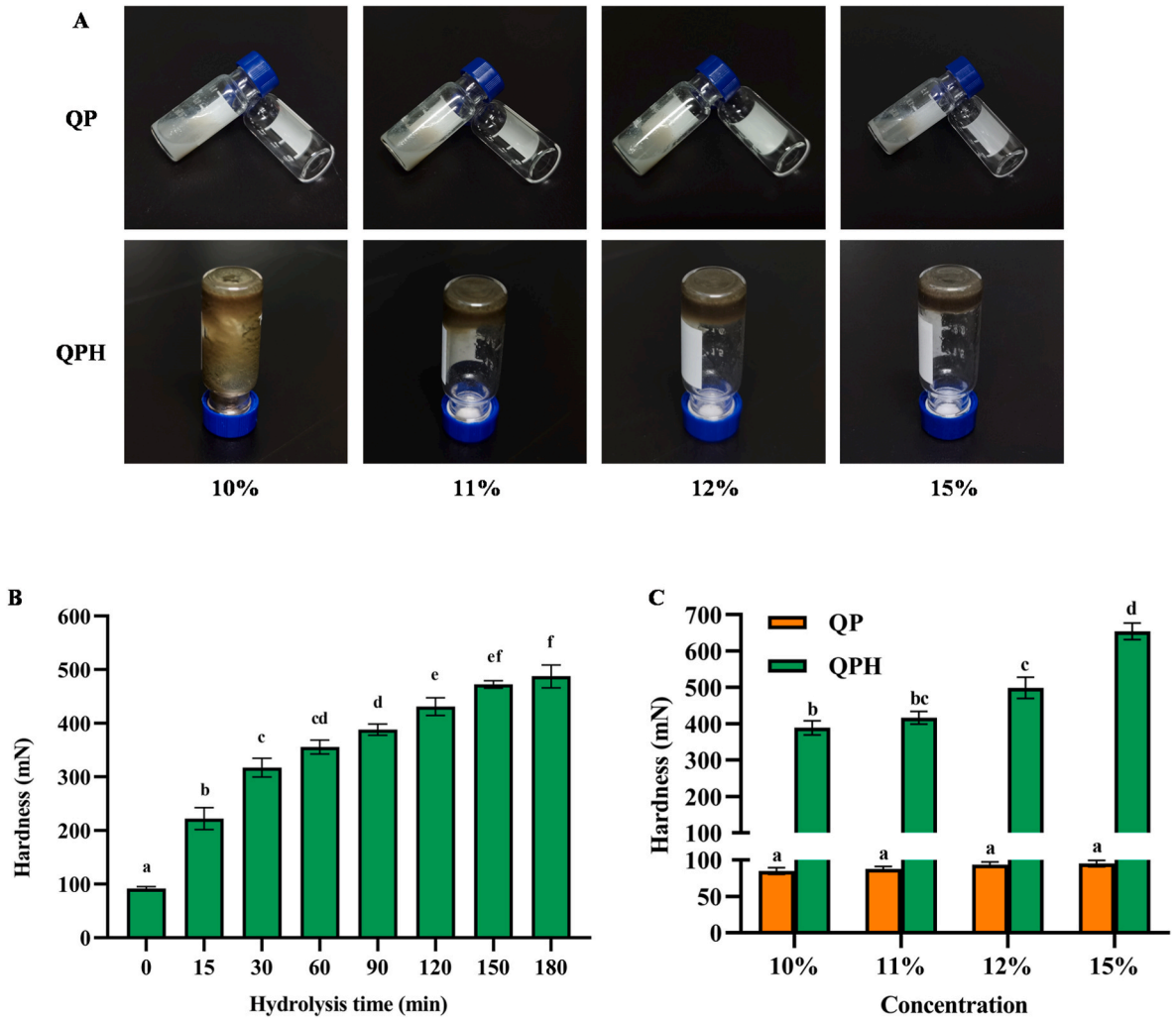

Fig. 2. Hardness of hydrogel/hydrosol formed by QP and QPH at various concentrations. (A) hydrogel forming ability; (B) changes in the hardness of 12% QP hydrogel with alcalase hydrolysis time; (C) hardness of 10%-15% QP (orange bars) and 10%-15% QPH (green bars). Mean value of three determinations ± SD, and values with different letters are significantly different ($p < 0.05$).

3.3. Rheological properties of QPH hydrogels

Rheological properties can directly reflect the formation and transformation of hydrogel structure, thereby facilitating the exploration of the mechanism of gel formation. For the viscosity test, both QP and QPH displayed an increasing trend as the sample concentration increased from 10% to 15%, whereas the viscosity of all samples decreased at each concentration with an increasing shear rate (0.1–100 s^{-1}) (Fig. 3A and B). Moreover, we found that all QPH samples exhibited a higher viscosity than QP samples at each share rate, implying that the structure of QP itself could not occur in sol-to-gel transition, whereas the structure of QPH generated by enzymatic degradation was more prone to interaction.

The values of G' and G'' were used to indicate the viscoelasticity of materials, indicating whether they behaved as an elastic solid ($G' > G''$) or as a viscous liquid ($G' < G''$). As shown in Fig. 3C and D, the frequency sweep test was conducted at 1% strain within the Linear Viscoelastic Region. For all QP samples at each concentration, the G' value was lower than the G'' value throughout the entire frequency range (0.1–100 Hz), and both G' and G'' values slightly increased as the frequency increased (Fig. 3C). Moreover, the G' values of all QP samples were lower than 10 Pa. These observations indicated that QP was weak in gelation properties and more inclined to exhibit fluid properties as hydrosol. In contrast, there were completely different trends between G' and G'' at each QPH concentration with increasing frequency. For 10% QPH, similar to the QP samples, its G' value was lower than the G'' value, but the difference between them was narrowed (Fig. 3D). When the concentration of QPH reached 11%, the gap between G' and G'' shrunk, and as the frequency increased, the G' value exceeded the G'' value, implying that 11% was the critical concentration for the sol-to-gel transition of QPH. Furthermore, the G' value thoroughly surpassed the G'' value as the concentration of QPH reached 12% or 15%, indicating that elasticity was dominant in the QPH structure. Similar results, regarding the viscoelasticity of protein, have been reported in previous studies (Luo, Cheng, Zhang, & Yang, 2022; Yu et al., 2022).

Nevertheless, QPH presented a fluid behaviour that is also characteristic of some concentrated macromolecular solutions. Moreover, when the concentration of macromolecular solutions reaches a certain value, the G' value will also be higher than the G'' value. As reported by a previous study, during the sol-gel transition, the construction of tridimensional structures led to gel formation. This behaviour is general because the viscoelastic properties of chemical and physical gels follow a power law near the critical gel point. The critical point could be clearly defined using exponential interpolation of the power law equations linking G' and G'' and results accord well with those obtained from the phase angle δ (Michon, Cuvelier, & Launay, 1993). Therefore, the loss tangent ($\tan\delta = G''/G'$) of samples at different concentrations in the frequency range (0.1–100 Hz) was calculated. For all samples, "tan δ <

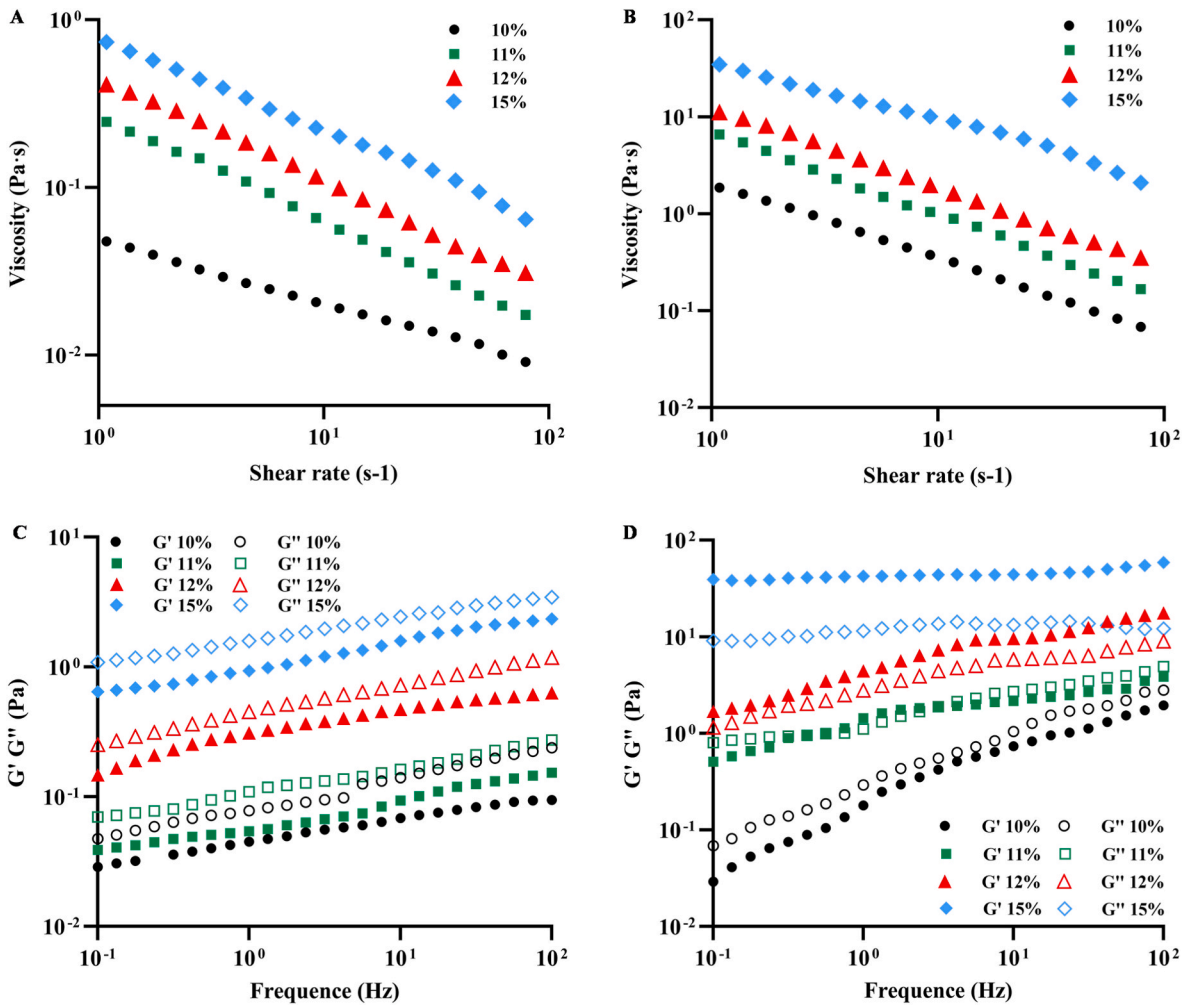

Fig. 3. Rheological properties of QP and QPH at various concentrations (10%-15%). Viscosity profile of QP (A) and QPH (B); storage modulus (G') and loss modulus (G'') of QP (C) and QPH (D).

1" decisively reflected the solid state of the samples, whereas "tan δ > 1" indicated a liquid state of the samples (Fu, Wu, & Su, 2021; Michon et al., 1993). The results were shown in Figs. S1A–B, the tan δ of QP at each concentration (10%–15%) was greater than 1 throughout the tested frequency range. However, at a certain frequency, the tan δ of QPH declined with the increase in QPH concentration. When QPH concentration rose to 11%, the tan δ of QPH was around 1, indicating the current concentration was the critical point of QPH. Moreover, it was obvious that 12% and 15% QPH had tan δ lower than 1. These results imply that the structure of QP itself might prevent the transition from sol to gel, while QP hydrolysis resulted in facile interaction in the peptide structure, which indicates a stable hydrogel network was formed of QP hydrolysis and corresponds with the results of hardness observation.

Furthermore, the enhanced gel strength may be due to the smaller particle size and unfolded protein structure, which improves the interactions between proteins or peptide molecules. Moreover, non-covalent bonds, including hydrogen bonds, disulfide bonds, and hydrophobic interactions, can influence the formation of plant protein gels (Galante, et al., 2020; Luo, Zhang, Palmer, Hemar, & Yang, 2021).

3.4. Microstructure analysis

Particle size is one of the main factors that affect the functional properties of proteins (Wang, et al., 2022). The particle size distribution and mean particle size are shown in Fig. 4A. The mean particle size of QP suspension was 46.25 μm, and its particle size distribution ranged from 2.35 to 677.70 μm. QP suspensions without treatment displayed large aggregates ranging from 0.06 to 100 μm, consistent with the QP sample in the present study (Shen, et al., 2021). After alcalase hydrolysis, the mean particle size of QPH was decreased than that of QP. However, the particle size distribution of QPH revealed a bimodal distribution. Most of the particles were in the 0.51–112.47 μm, with a smaller distribution between 148.26 and 778.1 μm. A previous study indicated that enzymatic hydrolysis could disrupt the intermolecular interactions of proteins and change the protein structure, thereby changing the aggregated state and particle size of protein (Ma, et al., 2022). However, excessive enzymatic hydrolysis or ultrasound treatment could lead to the interaction between exposed active groups, which may cause the reaggregation of protein/peptide molecules and an increase in particle size (C. Zhao et al., 2021).

SEM was performed to visually assess the network gel structure and particle shape of 12% QP and QPH. As illustrated in Fig. 4B, QP hydrogel displayed irregular and compactly stacked lamella, suggesting that it may be less capable of entrapping water molecules through hydrogen bonds. Moreover, the lamella surface was smooth with swelling protrusions stretching out, and there were also some protein particles on the lamellar surface. These results imply that the cross-linking of QP hydrogel is limited. In contrast, a regular, uniform, and interconnected porous structure was observed in the SEM image of QPH hydrogel. Meanwhile, its cavity wall thickness was very thin, and there were holes in the connection of adjacent cavities, with little or no protrusions and protein particles linked to the cavity wall. This change might be caused

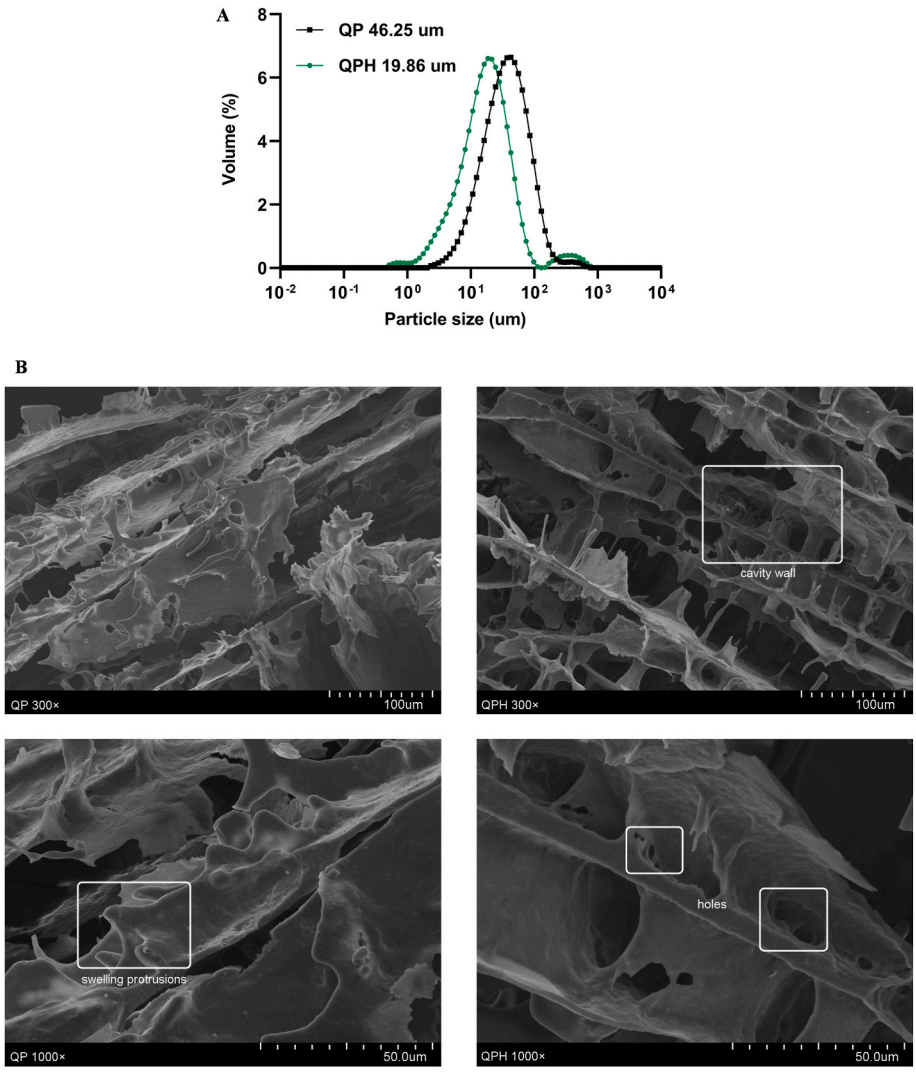

Fig. 4. (A) Particle size distributions of QP and QPH; (B) SEM images of 12% QP and 12% QPH hydrogels; the upper panel represent pictures at 300× magnification and the lower panel represent pictures at 1000× magnification; the white words represent the structure in the white box.

by the hydrolysis effect of alcalase, as mentioned previously, which decreased the particle size and resulted in the exposure of SH groups and hydrophobic groups (Yu, et al., 2022). These results indicate that QPH could form a strong self-assembled hydrogel and have a potent ability to capture water molecules through hydrogen bonds. Furthermore, the microstructural changes between QP and QPH are related to the functional properties, which is consistent with our results of gel hardness, rheological properties, and particle size.

3.5. Amino acid and proteomics analysis of QPH hydrogels

Amino acid composition, sequence, and spatial location are essential for the formation and properties of peptide hydrogels. In the present study, 17 different amino acids were detected in QPH (Supplemental Table 1), and previous studies have indicated that different amino acids contribute differently to the interactions between molecules. For QPH, the hydrophilic amino acids (Asp, Thr, Ser, Tyr, Glu, His, Lys, Arg, and Cys-Cys) made up 56.91%, and the hydrophobic amino acids (Leu, Ile, Phe, Gly, Ala, Val, Pro, and Met) made up 43.09%, suggesting that QPH represents an amphipathic nature and prefers to form aggregates spontaneously in solution, which was consistent with the results of surface hydrophobicity. Amino acid residues that could easily form hydrogen bonds because of the particular carboxyl, amino, or guanidyl groups were found among Asp, Glu, Lys, and Arg, accounting for 40.57% of the total amino acids (Yu, et al., 2022). Notably, the contents of Glu and Arg accounted for 13.85% and 10.17%, respectively. A previous study reported that the hydroxyl group of glutamic acid promoted the peptide-peptide interaction through hydrogen bonds, and the guanidine side group facilitated the interaction among peptide chains through hydrogen bonds, electrostatic interactions, and salt bridges, which ultimately alters the topology of the network formed and the final mechanical properties of the hydrogels (Gao, et al., 2017). Phe, Tyr, and His, which accounted for 11.56% of the total amino acids, were thought to contribute to peptide self-assembly due to the presence of phenyl rings or imidazole rings that can form π-π stacking (Yu, et al., 2022). In addition, it has been demonstrated that high helicity amino acids, particularly Ala and Leu, are considered to aid in stabilizing the network of peptide hydrogels. The high helicity amino acids possess a self-assembly tendency of α-helix structure, which could be triggered by hydrogen bonds to form a "coil-coil" multi-helix stable structure (Fu et al., 2021). In our study, over 10% of Ala and Leu were present in QPH.

Aside from the amino acid content, the effect of the peptide chain sequence of QPH on gel formation was investigated using ultra-high-performance liquid chromatography-tandem spectrometry. The data files were analyzed using the Andromeda scoring algorithm of MaxQuant software, along with the uniport-taxonomy_63,459 (*Chenopodium quinoa*). fasta database search. The identification results are summarized in Supplemental Tables 2 and a total of 97 peptide sequences were

identified in QPH. It was observed that 76 peptides have molecular weights greater than 1 kDa, with peptide chain length in the range of 9–25 residues and molecular weight in the range of 1016.49–2721.37 kDa, whereas the molecular weight of the remaining 19 peptides was less than 1 kDa, with peptide chain lengths ranging from 6 to 10 residues and molecular weight ranging from 613.34 to 997.62 kDa. These findings agree with those of a previous study (Yu, et al., 2022), implying that middle-length peptides that are similar to synthetic peptides (480 Da–6 kDa) contributed to hydrogel formation via self-assembly.

Protein electrostatic and hydrophobic interactions influence gelation behaviour. Whether the amphiphilic peptides displayed $(XZXZ)_n$ sequence of alternating hydrophobic (X) and hydrophilic (Z) residues or the peptides made up of alternating uncharged (U) and charged (C) residues known as the $(UCUC)_n$ sequence, both of which demonstrated potent gel aggregation capacity to self-assemble into hydrogels (Bowerman & Nilsson, 2012; Saiani et al., 2009). The analysis of the identified peptides revealed that QPH is primarily composed of amphipathic peptides and most of these identified peptides displayed the $(XZXZ)_n$ sequence in general, for instance, IGPQKPIPDVVVILPPKEDDVYAR, KLEPTPGDMIR, and RLNLEAVGVELDQTGAVK (Table 1). In total, 69 identified peptides with $(XZXZ)_n$ similar sequence comprised 33.33%–77.78% hydrophobic residues. In terms of the $(UCUC)_n$ sequence, a previous study reported that AEAEAKAKAEAEAKAK (yeast Zuotin peptides), AEAKAEAK, and FEFKFEFK (synthesized peptides) could obtain the robust gel aggregation capability through self-assembly (Saiani, et al., 2009). In this study, the charged residues of most peptides could reach or surpass 50% of total residues and presented a common sequence $(UCUC)_n$, for example, EDPKDDYLK, DLKEDPKDDYLK, and RMPDDLDYAK (Table 1). These observations suggest that the amino acid sequence and composition of QPH are critical for the final achievement of its hydrogel-forming ability, which may be attributed mostly to compliance with the hydrogel-forming rules of synthetic self-assembled peptides.

3.6. Molecular interactions of QPH aggregation

Previous studies have reported that enzymatic hydrolysis-induced changes in hydrophobicity and SH groups directly correlated with gel formation (G. Zhao et al., 2011). In our study, the surface hydrophobicity and free sulfhydryl content were determined and displayed in Fig. 5. The hydrophobicity of QP and its hydrolysates increased from 477 (QP) to 645 (QPH). The hydrophobicity of the 150-min hydrolysate was close to that of QPH, implying that the hydrophobic groups buried in QP were gradually exposed to enzymatic hydrolysis, and the exposure of the hydrophobic groups almost reached the maximum at 150 min. Conversely, the content of SH groups decreased with increasing DH, reaching a final value of 7.09 μmol/g. However, during the first 15 min, the concentration of SH groups was increased from 10.65 μmol/g of QP to 16.78 μmol/g of 15-min hydrolysate. Afterwards, the SH groups exhibited a continuous reduction from 16.78 μmol/g to 7.09 μmol/g of QPH. Similar results were also observed in a previous study, where the content of free SH groups of QP elevated from 10.9 μmol/g to 17.7 μmol/g at pH 8.5 during the first 5 min (Mäkinen, Zannini, Koehler, & Arendt, 2016), which suggested that enzymatic hydrolysis not only broke down proteins into short peptides but also disulfide bonds in the initial stage. These peptides may re-aggregate because of the

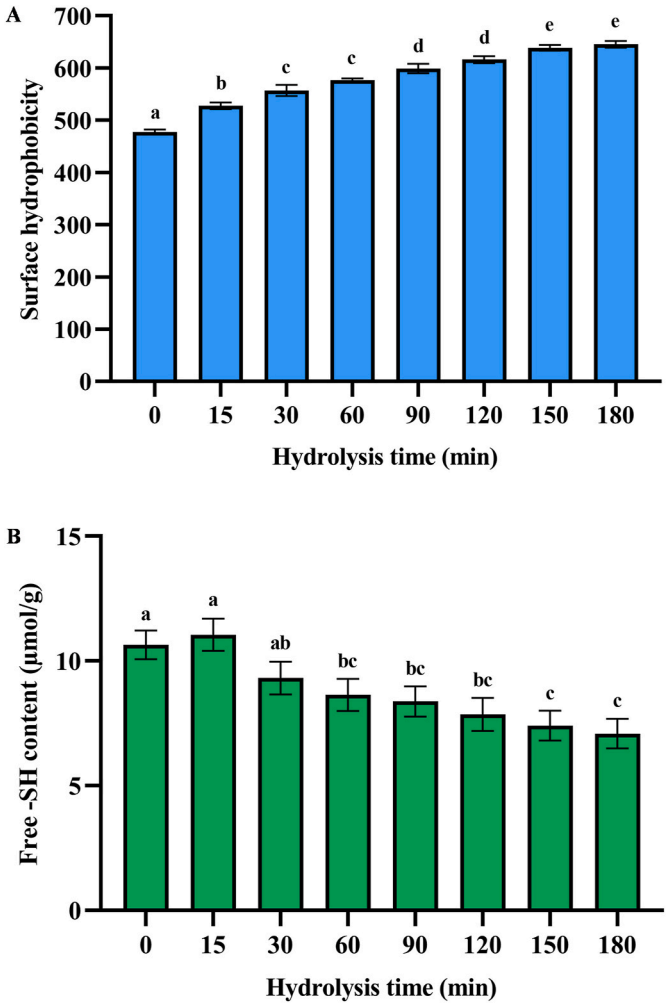

Fig. 5. Surface hydrophobicity (A) and free sulphydryl content (B) of QP and QPH samples. Mean value of three determinations ± SD, and values with different letters are significantly different ($p < 0.05$).

Table 1
Representative peptides identified in QPH.

Feature	Peptide sequence	m/z	Mass (Da)	Protein accession	Position
$(XZXZ)_n$	IGPQKPIPDVVVILPPKEDDVYAR	886.83	2657.48	A0A803MWB7	198–221
	KLEPTPGDMIR	636.83	1271.65	A0A803KU86	330–340
	RLNLEAVGVELDQTGAVK	638.02	1911.04	A0A803MUE8	302–320
	LEPLPDGSMNPK	657.32	1312.63	A0A803L2M5	1041–1052
	TIYIPQPTWGNHPK	826.43	1650.85	A0A803LBT5	213–226
	TPSPGIEIPEEWSAAAYTIAKSFTR	454.57	2721.37	A0A803M3Y3	10–34
$(UCUC)_n$	EDPKDDYLK	561.77	1121.52	A0A803KXN1	164–172
	DLKEDPKDDYLK	493.58	1477.73	A0A803KXN1	161–172
	RMPDDLDYAK	612.29	1222.57	A0A803M3Q4	133–142
	KPDTDFDFYK	638.30	1274.58	A0A803MPE1	406–415
	NLDDTIDDDKLK	702.85	1403.68	A0A803LGZ0	292–303
	KSMDDPGR	905.41	904.41	A0A803M212	540–547

The letters marked in shades represent hydrophobic amino acids, underlines represent positively charged amino acids, and wavy lines represent negatively charged amino acids.

interactions of exposed reactive groups, which are considered to contribute to the self-aggregation forming capacity and formation of the mesh-like structure of QPH. Furthermore, zeta potential was measured, and the zeta potential of QPH (−23.40 mV) was significantly lower than that of QP (−17.35 mV). A highly negative zeta potential is conducive to gel formation and stability (Yu, et al., 2022).

FTIR measurements were performed to further investigate the self-assembled ability of QPH. The FTIR spectra of QP and QPH are presented in Fig. 6, and both exhibited the typical FTIR absorbance spectrum of the protein. The characteristic peaks of QP appeared at 3293 cm^{-1} (amide A), 2961 cm^{-1}, 2931 cm^{-1} (amide B), 1656 cm^{-1} (amide I), 1542 cm^{-1} (amide II), and 1240 cm^{-1} (amide III). However, after hydrolysis treatment with alcalase, the same characteristic peaks of QPH were shifted to 3294 cm^{-1}, 2959 cm^{-1}, 2928 cm^{-1}, 1651 cm^{-1}, 1547 cm^{-1}, and 1243 cm^{-1}. Amide A represented the O–H and N–H stretching vibrations (Yu, et al., 2022), and it was found that the major peaks at 3293 cm^{-1} differed between QP and QPH. In particular, the relative intensity of the absorption peak of QPH at 3371 cm^{-1} was lower than that of QP. Moreover, the band at 1656 cm^{-1} (amide I) for the C═O stretching vibration of QP shifted to a lower frequency at 1651 cm^{-1} of QPH (Daliri, et al., 2021). Generally, the bands at amide A and amide I are mainly mixed peaks of chemical bonds subject to hydrogen bonding and non-hydrogen bonding, and the absorption peaks of chemical bonds are affected by hydrogen bonds shifting to the lower band (Liang, et al., 2022). Therefore, the change of the peaks at 3371 cm^{-1} indicated that the hydrogen bonding of QPH was stronger than that of QP, improving the gelation ability of QPH.

Fourier self-deconvolution (FSD) method was conducted in the amide I region (1700–1600 cm^{-1}) to analyze the secondary structure of quinoa peptides, and the proportions of α-helix, β-sheet, β-turn, and the random coil were calculated. As depicted in Fig. 6, compared with QP, the contents of α-helix and β-sheet were similar, whereas the random coil content increased significantly, and the β-turn content decreased in QPH, implying that enzymatic hydrolysis did affect the secondary structure of QP. Similarly, a previous study found that the contents of α-helix and β-sheet were decreased, whereas the random coil content increased after alcalase hydrolysis (Ma, et al., 2022). Moreover, α-helix, β-turn, and β-sheet relied on specific forms of hydrogen bond interactions to form a relatively ordered structure, whereas random coil had a disordered structure because of the differences in hydrogen bond interactions (Xu & Wang, 2019). In our study, the breakage of the peptide and disulfide bonds of QP under alcalase treatment caused α-helix, β-turn, and β-sheet to unfold and form a random coil structure, resulting in an increased disordered secondary structure and exposed reactive groups of QPH. Overall, the enzymatic hydrolysis of QPH increased the disordered secondary structure and exposure of hydrogen-bonded groups, which had a significant effect on the formation of self-assembling peptide hydrogels. However, the self-assembly mechanism of QPH peptides requires further investigation.

4. Conclusions

Our study described a method for producing spontaneous self-assembly peptides with hydrogel-forming capability from quinoa proteins using moderate enzyme hydrolysis without the use of hazardous chemicals or crosslinkers. Moreover, the experiment results revealed that alcalase hydrolysis significantly affected the structure and gel-forming properties of quinoa proteins. Quinoa peptides generated by hydrolysis were observed with a Mw of 5.01 kDa and could self-assemble into hydrogels with favourable physical and rheological properties, resulting from changes in the driving forces such as hydrophobic aggregation and hydrogen bonding. Furthermore, the amino acid analysis

A

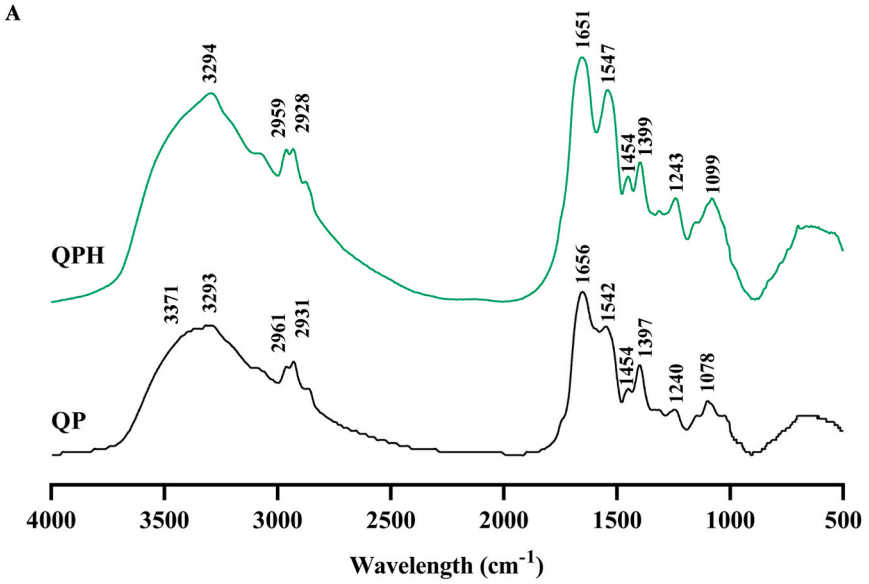

B

	β-sheet (%)	Random (%)	α-helix (%)	β-turn (%)
QP	27.64 ± 0.47 [a]	24.63 ± 0.74 [b]	15.82 ± 0.55 [a]	31.91 ± 0.88 [a]
QPH	27.36 ± 1.26 [a]	27.09 ± 1.10 [a]	15.61 ± 1.02 [a]	29.94 ± 1.11 [b]

Fig. 6. FTIR spectroscopy (A) and secondary structures (B) of QP and QPH. Mean value of three determinations ± SD, and values with different letters in the same column are significantly different ($p < 0.05$).

revealed that amino acids such as Arg and Glu contribute to forming self-assembled hydrogels. Proteomics analysis indicated that most identified quinoa peptides possessed the typical molecular properties of self-assembled peptides (including peptides with alternate charged and uncharged residues) and amphiphilic peptides (composed of alternate hydrophilic and hydrophobic residues). Our study proposed a simple, low-cost, efficient, and environmentally friendly technique for the large-scale manufacture of plant-based self-assembled hydrogels in factories, as well as a novel idea for the system that has long relied on synthetic peptides to produce peptide hydrogels. However, neither the quinoa variety nor the synergistic effects of multiple enzymes were considered in our study. Therefore, future work should further investigate the effects of various quinoa protein types and enzyme combinations on the characteristics of quinoa peptide hydrogels.

CRediT authorship contribution statement

Xin Fan: Conceptualization, Methodology, Investigation, Data curation, Formal analysis, Writing - original draft. **Huimin Guo**: Formal analysis, Methodology, Writing - review & editing. **Aurore Richel**: Supervision, Writing - review & editing. **Lizhen Zhang:** Writing - review & editing. **Chenghong Liu**: Resources, Funding acquisition. **Peiyou Qin**: Project administration, Resources, Writing - review & editing. **Christophe Blecker**: Conceptualization, Supervision, Writing - review & editing. **Guixing Ren**: Funding acquisition, Project administration, Supervision, Writing - review & editing.

Declaration of competing interest

The authors declare that they have no known competing financial interests or personal relationships that could have appeared to influence the work reported in this paper.

Data availability

Data will be made available on request.

Acknowledgements

This work was supported by the Agricultural Science and Technology Innovation Program of the Chinese Academy of Agricultural Sciences (Grant No. CAAS-ASTIP-2022-ICS), Shanghai Pujiang Program (22PJD066), Shanghai "Science and Technology Innovation Action Plan" (22015810100), a postgraduate international exchange grant from the Chinese Academy of Agricultural Sciences and the China Scholarship Council (CSC). The authors would also like to thank Nicolas Jacquet, Lynn Doran and Marjorie Servais from the Teaching and Research Center, Gembloux, Belgium, for their guidance in this study.

Appendix A. Supplementary data

Supplementary data to this article can be found online at https://doi.org/10.1016/j.foodhyd.2023.109139.

References

Abugoch, L. E., Romero, N., Tapia, C. A., Silva, J., & Rivera, M. (2008). Study of some physicochemical and functional properties of quinoa (Chenopodium quinoa willd) protein isolates. *Journal of Agricultural and Food Chemistry, 56*(12), 4745–4750. https://doi.org/10.1021/jf703689u

Beveridge, T., Toma, S. J., & Nakai, S. (1974). Determination of SH- and SS-groups in some food proteins using Ellman's Reagent. *Journal of Food Science, 39*(1), 49–51. https://doi.org/10.1111/j.1365-2621.1974.tb00984.x

Bowerman, C. J., & Nilsson, B. L. (2012). Review self-assembly of amphipathic β-sheet peptides: Insights and applications. *Peptide Science, 98*(3), 169–184. https://doi.org/10.1002/bip.22058

Brinegar, C., & Goundan, S. (1993). Isolation and characterization of chenopodin, the 11S seed storage protein of quinoa (Chenopodium quinoa). *Journal of Agricultural and Food Chemistry, 41*(2), 182–185. https://doi.org/10.1021/jf00026a006

Brinegar, C., Sine, B., & Nwokocha, L. (1996). High-cysteine 2S seed storage proteins from quinoa (Chenopodium quinoa). *Journal of Agricultural and Food Chemistry, 44*(7), 1621–1623. https://doi.org/10.1021/jf950830+

Chen, D., & Campanella, O. H. (2022). Limited enzymatic hydrolysis induced pea protein gelation at low protein concentration with less heat requirement. *Food Hydrocolloids, 128*, Article 107547. https://doi.org/10.1016/j.foodhyd.2022.107547

Daliri, H., Ahmadi, R., Pezeshki, A., Hamishehkar, H., Mohammadi, M., Beyrami, H., et al. (2021). Quinoa bioactive protein hydrolysate produced by pancreatin enzyme-functional and antioxidant properties. *Lebensmittel-Wissenschaft & Technologie, 150*, Article 111853. https://doi.org/10.1016/j.lwt.2021.111853

De Leon Rodriguez, L. M., & Hemar, Y. (2020). Prospecting the applications and discovery of peptide hydrogels in food. *Trends in Food Science & Technology, 104*, 37–48. https://doi.org/10.1016/j.tifs.2020.07.025

Elsohaimy, S. A., Refaay, T. M., & Zaytoun, M. A. M. (2015). Physicochemical and functional properties of quinoa protein isolate. *Annals of Agricultural Science, 60*(2), 297–305. https://doi.org/10.1016/j.aoas.2015.10.007

Fu, K., Wu, H., & Su, Z. (2021). Self-assembling peptide-based hydrogels: Fabrication, properties, and applications. *Biotechnology Advances, 49*, Article 107752. https://doi.org/10.1016/j.biotechadv.2021.107752

Galante, M., De Flaviis, R., Boeris, V., & Spelzini, D. (2020). Effects of the enzymatic hydrolysis treatment on functional and antioxidant properties of quinoa protein acid-induced gels. *Lebensmittel-Wissenschaft & Technologie, 118*, Article 108845. https://doi.org/10.1016/j.lwt.2019.108845

Gao, J., Tang, C., Elsawy, M. A., Smith, A. M., Miller, A. F., & Saiani, A. (2017). Controlling self-assembling peptide hydrogel properties through network topology. *Biomacromolecules, 18*(3), 826–834. https://doi.org/10.1021/acs.biomac.6b01693

Gosal, W. S., & Ross-Murphy, S. B. (2000). Globular protein gelation. *Current Opinion in Colloid & Interface Science, 5*(3), 188–194. https://doi.org/10.1016/S1359-0294(00)00057-1

Liang, R., Zhang, H., Wang, Y., Ye, J., Guo, L., He, L., et al. (2022). Dual dynamic network system constructed by waterborne polyurethane for improved and recoverable performances. *Chemical Engineering Journal, 442*, Article 136204. https://doi.org/10.1016/j.cej.2022.136204

Luo, L., Cheng, L., Zhang, R., & Yang, Z. (2022). Impact of high-pressure homogenization on physico-chemical, structural, and rheological properties of quinoa protein isolates. *Food Structure, 32*, Article 100265. https://doi.org/10.1016/j.foostr.2022.100265

Luo, L., Zhang, R., Palmer, J., Hemar, Y., & Yang, Z. (2021). Impact of high hydrostatic pressure on the gelation behavior and microstructure of quinoa protein isolate dispersions. *ACS Food Science & Technology, 1*(11), 2144–2151. https://doi.org/10.1021/acsfoodscitech.1c00332

Mäkinen, O. E., Zannini, E., Koehler, P., & Arendt, E. K. (2016). Heat-denaturation and aggregation of quinoa (Chenopodium quinoa) globulins as affected by the pH value. *Food Chemistry, 196*, 17–24. https://doi.org/10.1016/j.foodchem.2015.08.069

Ma, Z., Li, L., Wu, C., Huang, Y., Teng, F., & Li, Y. (2022). Effects of combined enzymatic and ultrasonic treatments on the structure and gel properties of soybean protein isolate. *Lebensmittel-Wissenschaft & Technologie, 158*, Article 113123. https://doi.org/10.1016/j.lwt.2022.113123

McClements, D. J., Newman, E., & McClements, I. F. (2019). Plant-based milks: A review of the science underpinning their design, fabrication, and performance. *Comprehensive Reviews in Food Science and Food Safety, 18*(6), 2047–2067. https://doi.org/10.1111/1541-4337.12505

Nieto-Nieto, T. V., Wang, Y. X., Ozimek, L., & Chen, L. (2014). Effects of partial hydrolysis on structure and gelling properties of oat globular proteins. *Food Research International, 55*, 418–425. https://doi.org/10.1016/j.foodres.2013.11.038

Ruiz, G. A., Xiao, W., van Boekel, M., Minor, M., & Stieger, M. (2016). Effect of extraction pH on heat-induced aggregation, gelation and microstructure of protein isolate from quinoa (Chenopodium quinoa Willd). *Food Chemistry, 209*, 203–210. https://doi.org/10.1016/j.foodchem.2016.04.052

Saiani, A., Mohammed, A., Frielinghaus, H., Collins, R., Hodson, N., Kielty, C. M., et al. (2009). Self-assembly and gelation properties of α-helix versus β-sheet forming peptides. *Soft Matter, 5*(1), 193–202. https://doi.org/10.1039/B811288F

Shen, Y., Tang, X., & Li, Y. (2021). Drying methods affect physicochemical and functional properties of quinoa protein isolate. *Food Chemistry, 339*, Article 127823. https://doi.org/10.1016/j.foodchem.2020.127823

Wang, Y.-L., Yang, J.-J., Dai, S.-C., Tong, X.-H., Tian, T., Liang, C.-C., et al. (2022). Formation of soybean protein isolate-hawthorn flavonoids non-covalent complexes: Linking the physicochemical properties and emulsifying properties. *Ultrasonics Sonochemistry, 84*, Article 105961. https://doi.org/10.1016/j.ultsonch.2022.105961

Xu, K., & Wang, J. (2019). Discovering the effect of alum on UV photo-degradation of gelatin binder via FTIR, XPS and DFT calculation. *Microchemical Journal, 149*, Article 103934. https://doi.org/10.1016/j.microc.2019.05.034

Yang, Z., de Campo, L., Gilbert, E. P., Knott, R., Cheng, L., Storer, B., et al. (2022). Effect of NaCl and CaCl2 concentration on the rheological and structural characteristics of thermally-induced quinoa protein gels. *Food Hydrocolloids, 124*, Article 107350. https://doi.org/10.1016/j.foodhyd.2021.107350

Yin, S.-W., Tang, C.-H., Wen, Q.-B., & Yang, X.-Q. (2010). Functional and conformational properties of phaseolin (phaseolus vulgris L.) and kidney bean protein isolate: A comparative study. *Journal of the Science of Food and Agriculture, 90*(4), 599–607. https://doi.org/10.1002/jsfa.3856

Yu, M., Lin, S., Ge, R., Xiong, C., Xu, L., Zhao, M., et al. (2022). Buckwheat self-assembling peptide-based hydrogel: Preparation, characteristics and forming mechanism. *Food Hydrocolloids, 125*, Article 107378. https://doi.org/10.1016/j.foodhyd.2021.107378

Zhao, C., Chu, Z., Miao, Z., Liu, J., Liu, J., Xu, X., et al. (2021). Ultrasound heat treatment effects on structure and acid-induced cold set gel properties of soybean protein

isolate. *Food Bioscience, 39*, Article 100827. https://doi.org/10.1016/j.fbio.2020.100827

Zhao, G., Liu, Y., Zhao, M., Ren, J., & Yang, B. (2011). Enzymatic hydrolysis and their effects on conformational and functional properties of peanut protein isolate. *Food Chemistry, 127*(4), 1438–1443. https://doi.org/10.1016/j.foodchem.2011.01.046

Zuo, Z., Zhang, X., Li, T., Zhou, J., Yang, Y., Bian, X., et al. (2022). High internal phase emulsions stabilized solely by sonicated quinoa protein isolate at various pH values and concentrations. *Food Chemistry, 378*, Article 132011. https://doi.org/10.1016/j.foodchem.2021.132011